Langmuir

Article

pubs.acs.org/Langmuir

Smart Polymer Nanoparticles for High-Performance Water-Borne Coatings

Susana Piçarra,*[,‡,†] Alexandra Fidalgo,[§,†] Aleksander Fedorov,[†] José M. G. Martinho,[†] and José Paulo S. Farinha*[,†]

[†]IN-Institute of Nanoscience and Nanotechnology and Centro de Química-Física Molecular , Instituto Superior Técnico (Universidade de Lisboa), 1049-001 Lisboa, Portugal

[‡]Escola Superior de Tecnologia de Setúbal, Instituto Politécnico de Setúbal, Campus do IPS, Estefanilha, 2910-761 Setúbal, Portugal

[§]Universidade Europeia − Laureate International Universities, Quinta do Bom Nome, Estrada da Correia, 53-1500-210 Lisboa, Portugal

Supporting Information

ABSTRACT: Poly(butyl methacrylate) nanoparticles encapsulating a silica precursor, tetraethoxysilane (TEOS), were synthesized by a two-step emulsion polymerization process. We show that TEOS remains mostly unreacted inside the nanoparticles in water but acts both as a plasticizer and cross-linker in films cast from the dispersions. The diffusion-enhancing plasticizing effect is dominant at annealing temperatures closer to the glass-transition temperature of the polymer, and sol−gel cross-linking reactions predominate at higher temperatures. By choosing an appropriate annealing temperature, we were able to balance polymer interdiffusion and silica cross-linking to obtain films with good mechanical properties and excellent chemical resistance. The hybrid cross-linked films produced from these novel "smart" nanoparticles can be used in water-borne environmentally friendly coatings for high-performance applications.

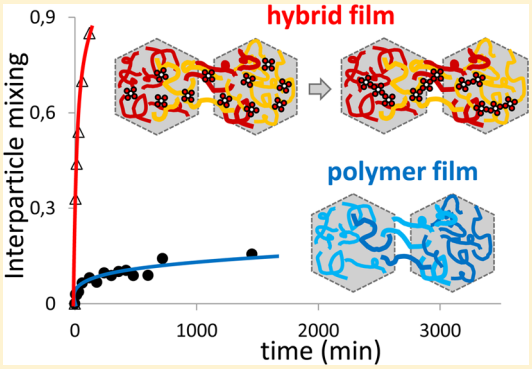

1. INTRODUCTION

The coatings industry has suffered a strong remaking over the last decades, mostly motivated by environmental concerns.[1] To reduce the emission of volatile organic compounds (VOCs), solvent-borne coatings have been replaced by water-based alternatives composed of water dispersions of submicrometer-size polymer particles (also known as latex dispersions). To prepare films, the dispersions are cast and dried. As water evaporates, the polymer particles come into contact and deform in a process driven by both the polymer−air surface tension and capillarity forces.[2,3] After drying, the weak adhesion at the interparticle boundaries is due to van der Waals interactions between polymer chains from neighboring particles and eventually hydrogen bonding and/or ion-pairing interactions between functional groups at the particle surfaces, which originate films with very poor mechanical properties. These properties can be substantially enhanced through polymer diffusion across the interparticle boundaries[4−6] at temperatures well above the polymer glass-transition temperature (T_g). Coalescing aid agents are frequently added to plasticize the chains and decrease T_g, but this increases the VOC content of the coating formulations.[5]

Further improvements are thus still needed, not only to achieve the long-desired zero-VOC content but also to reach the same level of performance as solvent-borne coatings needed for high-performance applications as in the automotive and aerospace industries.

Several strategies have been used to improve the performance of water-borne coatings, such as the introduction of inorganic fillers and the addition of reactive monomers.[4] To obtain a film with good mechanical strength, the length over which the chains diffuse has to be comparable to their radius of gyration,[7,8] or in the case of reactive blends, chain cross-linking has to occur on both sides of the interface between nanoparticles.[9,10] Thus, latex particles bearing functional groups that react to form cross-links are frequently used to improve film toughness and to provide solvent resistance.[11] The most common cross-linker agents in aqueous latex dispersions are based on epoxy, *N*-methylolamide, N-isobutoxymethylamide, and acetoacetyl groups. Some of these groups self-react under appropriate conditions (epoxy or *N*-methylolamide) whereas others require an external multifunctional reactant to form the required cross-links.[12]

The design of reactive latexes is, however, very challenging, as cross-links often retard or even suppress chain interdiffusion. Liu et al. studied the effect of long-chain branches and cross-

Received: December 23, 2013
Revised: September 18, 2014
Published: September 23, 2014

   dx.doi.org/10.1021/la502826r | *Langmuir* 2014, 30, 12345−12353

links on the rate of polymer interdiffusion in films.[13] Aradian et al. developed a theoretical model for the competition between chain interdiffusion and cross-linking reactions at polymer interfaces, considering three main regimes: (i) when the reaction is much slower than interdiffusion, leading to complete interfacial healing before significant gel development (the properties of the obtained film are very similar to the bulk material); (ii) when reaction and interdiffusion have comparable rates, yielding a nonequilibrium interface (a substantial number of cross-links is developed and the mean chain length between cross-links spans the interface); and (iii) when the reaction is much faster than diffusion and no cross-linked chains bridge the interface (adhesion is entirely due to dangling chain ends that diffuse after the reaction is completed, a situation similar to the case of films formed from pre-cross-linked latex particles with poor mechanical properties).[9,14]

Although the polymer diffusion rate for linear chains mostly depends on the temperature and chain length, cross-links introduce branches in the polymer chains that decrease their diffusion rate and originate networks, which ultimately cease polymer diffusion.[12] Therefore, to obtain films with good mechanical performance and chemical resistance, the cross-linking reactions have to occur to a large extent, but only after substantial polymer mixing across the particle boundaries.[14,16]

There are a number of strategies to introduce reactive groups into water-borne coating formulations, namely,[14,15] (i) the dissolution of polymers containing reactive functionalities in organic solvents followed by emulsification in water; (ii) the copolymerization of reactive functionalities into latex particles during emulsion polymerization and the introduction of an external cross-linker immediately before application to the substrate; and (iii) latex blends containing reactive groups confined within separate particles that can only cross-link after chain interdiffusion between adjacent particles.

In this work, we developed novel reactive poly(*n*-butyl methacrylate-*co*-methacrylic acid) particles containing a significant amount of encapsulated tetraethoxysilane (TEOS) that acts both as a plasticizer and cross-linker. To our knowledge, this is the first time that reactive molecules are introduced inside latex particles without being copolymerized into the chains. By buffering the dispersion at neutral pH, we avoided the hydrolysis and condensation of the encapsulated TEOS[17] before film formation so that most TEOS remained unreacted inside the hydrophobic polymer particles and the dispersions were stable for very long times. During film formation, TEOS can act both as a plasticizer (promoting chain interdiffusion) and as a cross-linker (leading to the formation of a hybrid organic−inorganic network). By tuning the annealing temperature in order to balance diffusion and reaction, it is possible to obtain hybrid films with excellent healing properties and chemical resistance.

2. MATERIALS AND METHODS

2.1. Materials. Tetraethoxysilane (TEOS, Aldrich, 98%), ethylene glycol dimethacrylate (EGDMA, Aldrich, 98%), 1-dodecanethiol (DDTh, Aldrich, 98+%), potassium persulfate (KPS, Aldrich, 99+%), and sodium dodecyl sulfate (SDS, Sigma, 99% GC grade) were used as received. *n*-Butyl methacrylate (BMA, Aldrich, 99%) and methacrylic acid (MAA, Aldrich, 99%) were distilled and kept under nitrogen before use. Tetrahydrofuran (THF, Aldrich, HPLC grade) was dried over CaH_2 (Sigma-Aldrich, ≥90%) and filtered through a 0.20 μm membrane when used for multiangle light scattering size exclusion chromatography (MALDI-SEC). The dyes, 4-(phenanthren-9-yl)butyl methacrylate (Phe) and 4-(anthracen-2-yl)butyl methacrylate (Ant), were synthesized as described previously.[18,19]

2.2. Latex Synthesis. Latex particles were synthesized from cross-linked PBMA nanoparticles in an emulsion, which were produced by introducing KPS (0.5905 g), SDS (2.3206 g), BMA (26.67 g), and EGDMA (0.8398 g) into a previously degassed 1 L glass reactor containing 560 mL of phosphate buffer (pH 7.00, ionic strength 40 mM). The mixture was stirred for 2 h at 260 rpm and 80 °C under nitrogen. The produced fully cross-linked particles were used as nanoreactors (NRs) to polymerize linear p(BMA-*co*-MAA) chains further and simultaneously encapsulate TEOS molecules. Thus, ca. 25 g of the NRs emulsion was introduced into a degassed 250 mL round-bottomed flask previously filled with nitrogen and mechanically stirred at 210 rpm. Polymerization proceeded at 80 °C under starved feed conditions by continuously adding both an aqueous buffered solution (pH 7.00, ionic strength 0.04 mM) at a rate of 0.0375 mL/min (with KPS and SDS) and an organic phase at 0.0573 mL/min (constituted by a mixture of BMA, TEOS, MAA, DDTh, and one of the dye-labeled monomers, Ant or Phe, when necessary). Both aqueous and organic phases were degassed before addition. The reactions proceeded for 7 h.

Finally, SDS and other free ionic species were removed from the emulsions by diluting and stirring all latex samples in the presence of a AG 501-X8 mixed-bed resin from Bio-Rad (20−50 mesh) for 2 h and filtering. All latexes (both model and hybrid latexes) remained stable in emulsion for several months. (See long term stability of the hybrid particles in the Supporting Information.) Both control and hybrid nanoparticles were prepared following this procedure, either unlabeled (NP and NPT) or dye-labeled with Ant (*A*-NP and *A*-NPT) or Phe (*P*-NP and *P*-NPT). The recipes are given in Table S1 (Supporting Information).

2.3. Particle Characterization. Particle sizes and size distributions were measured by dynamic light scattering (DLS) in a Brookhaven Instruments BI-200SM goniometer and BI-9000AT correlator using a He−Ne laser (632.8 nm, 35 mW, model 127, Spectra Physics) and an avalanche photodiode detector. The measurements were carried out in glass cylindrical cells in order to simplify the corrections needed for refractive index variations. The circular vat cell contained decaline to minimize light refraction. The DLS data were analyzed using the analysis package CONTIN and a cumulant expansion (from Brookhaven) to determine the translational diffusion coefficient,[20] from which the hydrodynamic radius (R_h) of the particles was calculated using the Stokes−Einstein equation for noninteracting spheres.

The molecular weight and molecular weight distribution of the linear p(BMA-*co*-MAA) chains produced inside the NRs were determined by MALDI-SEC using two columns in series (Waters HR5 and Phenomenex 10^4) and THF as an eluent (0.8 mL/min). Three detectors (a Waters 470 fluorescence detector, a Waters 2410 refractive index detector, and a Wyatt miniDawn TREOS multiangle light scattering detector) were used. All emulsion samples were freeze-dried, dissolved in THF, and filtered (with a 0.20 μm membrane) prior to injection.

The solids content (SC wt %) was determined by weighing four samples of each emulsion before and after drying.

2.4. Film Preparation. Films were prepared by mixing phenanthrene- and anthracene-labeled particles in an emulsion (1:1 molar ratio) and by spreading the resulting mixtures on Parafilm. Films were allowed to dry inside a closed chamber saturated with water vapor at 30 °C, forming crack-free films. Once the films were dried, Parafilm was removed and each film was annealed at a given temperature (between 80 and 110 °C). Samples were taken out of the oven periodically and cooled to room temperature for fluorescence measurements.

2.5. Film Resistance to Solvents. Four thick films of roughly the same shape and dimensions were prepared from the emulsions containing unlabeled hybrid particles. All films were annealed for 90 min at 80, 90, 100, or 110 °C, individually weighed, and put on a 0.45 μm poly(tetrafluoroethylene) (PTFE) membrane of a Millipore filtration kit. They were washed for 45 min under vacuum with pure

Scheme 1. Cartoons Representing the Structures of the Produced Nanoparticles[a]

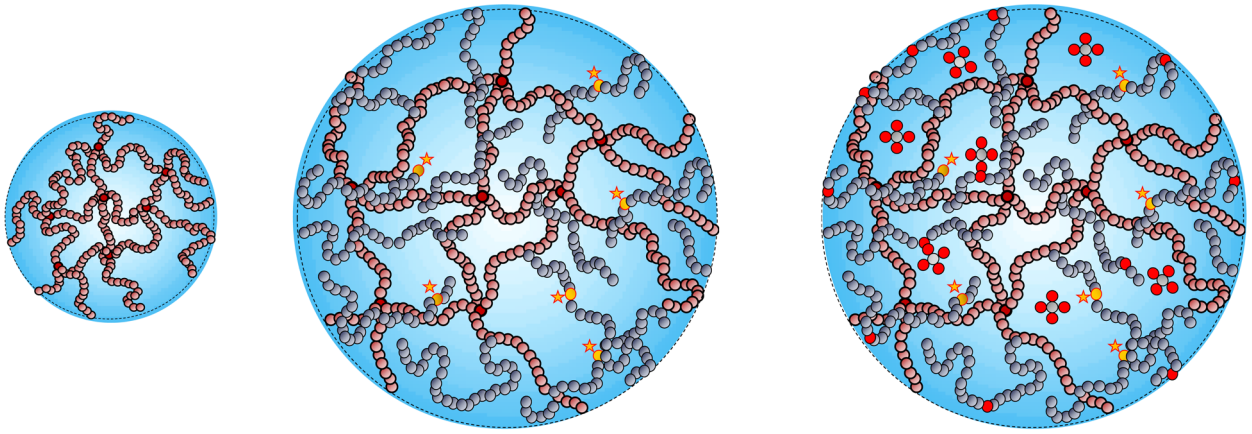

[a]Cross-linked PBMA nanoreactors (A); polymeric control nanoparticles (NP, *P*-NP, and *A*-NP) formed by a polymer gel swollen by linear polymer chains (B); and hybrid nanoparticles (NPT, *P*-NPT, and *A*-NPT) formed by a polymer nanogel swollen by linear chains and TEOS molecules (C). Phe/Ant-labeled co-monomers (yellow ★, yellow ●; MAA co-monomer (red ●); TEOS (red four-dot symbol with gray center); TEOS-MAA side group (red five-dot symbol with gray center).

THF (a very good solvent for PBMA). The films were then dried to constant weight. The fraction of the remaining macroscopic gel (RMG, wt %) corresponds to the ratio of the mass of the dried film at the membrane after washing to the mass of the initial film.

2.6. Film Characterization by TEM. TEM images and EADS analysis were obtained on a Hitachi transmission electron microscope (model H-8100 with a LaB6 filament) using an accelerator voltage of 200 kV. One drop of dispersion was placed on a carbon grid, dried at room temperature, and annealed at 100 °C before observation.

2.7. Film Characterization by IR Spectroscopy. Diffuse Reflectance Infrared Fourier-Transform (DRIFT) spectra of the dried films were recorded in a Mattson RS1 spectrometer, with a wideband MCT detector (400−4000 cm^{-1} spectral range) and a Graseby/Specac selector (with specular reflection blocker). The instrumental resolution was set at 4 cm^{-1}, and the final spectra resulted from 500 coadded scans for each sample divided by the same number of scans for the background (ground KBr, FTIR grade). The diffuse spectra were transformed to Kubelka-Munk units using the FIRST software. The samples were prepared by grinding a mixture of KBr and film, in appropriate weight proportions, to obtain spectral absorbance in the range of applicability of the Kubelka−Munk transformation.

2.8. Fluorescence Decay Measurements. Fluorescence decays were measured by the single-photon timing (SPT) technique. The system consists of a diode-pumped solid-state Nd:YVO_4 laser (Vanguard, Spectra Physics) delivering 2 W of 532 nm light at a 76 MHz repetition rate with a pulse duration of ∼12 ps, synchronously pumping a cavity-dumped dye laser (701-2, Coherent, delivering ∼40 nJ pulses of 5 to 6 ps at a 3.4 MHz repetition rate) working with rhodamine 6G. Intensity decay measurements were made by collecting both the impulses and decays with the emission polarizer set at the magic angle position. Impulses were recorded slightly away from the excitation wavelength at 295 nm with a scattering suspension. For the decays, a cutoff filter was effectively used to remove excitation light. Emission light passed through a depolarizer before reaching the Jobin-Yvon HR320 monochromator with a grating of 100 lines/mm, which selected the 350 nm fluorescence light from phenanthrene with a bandwidth of 6 nm. The fluorescence was detected by a Hamamatsu 2809U-01 microchannel plate photomultiplier. No less than 20 000 counts were accumulated at the maximum counts channel. The decay curves were analyzed using a nonlinear least-squares reconvolution method.[21] All of the fluorescence decay measurements were carried out at room temperature in free-standing films.

2.9. Förster Ressonance Energy Transfer (FRET) Analysis. Polymer diffusion was evaluated by measuring the extent of FRET between donor and acceptor dyes,[22] calculated from the fluorescence decay curves of the donor. The efficiency of energy transfer, $\Phi_{ET}(t)$, as a function of the annealing time, t, can be determined as

$$\Phi_{ET}(t) = \frac{1 - \int_0^\infty I_D(t, t')\,dt'}{\int_0^\infty I_D^0(t, t')\,dt'} \quad (1)$$

where the donor fluorescence decay with time t in the presence and absence of acceptors are represented by $I_D(t, t')$ and $I_D^0(t, t')$, respectively.

The evolution of Φ_{ET} as a function of the annealing time, t, can be used to calculate a normalized efficiency of energy transfer, f_m, which is related to the extent of polymer diffusion:[22]

$$f_m = \frac{\Phi ET(t) - \Phi_{ET}(0)}{\Phi_{ET}(\infty) - \Phi_{ET}(0)} \quad (2)$$

We consider that the f_m values are approximately proportional to the fraction of mass that has diffused across the interface,[22] where the efficiency of energy transfer for a fully mixed system, $\Phi_{ET}(\infty)$, was theoretically calculated.[18,23]

3. RESULTS AND DISCUSSION

3.1. Nanoparticle Synthesis. All nanoparticles were prepared from smaller cross-linked PBMA nanoreactors (NRs) produced by batch emulsion polymerization, as described before.[18] Characterization by DLS revealed that the NRs have a mean hydrodynamic diameter of D_h = 52.3 nm with a relative variance of 0.03, whereas MALDI-SEC measurements showed that these particles are fully cross-linked because no free chains were detected at high elution times.[18]

Both the copolymerization of BMA with 0.8 mol % MAA and the encapsulation of TEOS occurred inside the NRs, through a semicontinuous emulsion process. During this step no cross-linker was added, and linear p(BMA-*co*-MAA) chains were polymerized inside the NRs, swelling them. The formation of core−shell structures was prevented by the small dimensions of the seed nanoparticles.[24] The fluorescently labeled linear chains were synthesized using 1 mol % of a dye-labeled monomer

dx.doi.org/10.1021/la502826r | *Langmuir* 2014, 30, 12345−12353

(Phe for *P*-NP and *P*-NPT; Ant for *A*-NP and *A*-NPT; see Table S1, Supporting Information). Chain-transfer agent DDTh was always added during the nanoparticle synthesis to control the molecular weight of the linear chains. During the synthesis of the hybrid nanoparticles, TEOS and MAA were also added. However, while MAA polymerizes being incorporated into the linear polymer chains, the hydrophobic TEOS is only encapsulated in the particles. The partitioning of TEOS among the different phases present in the emulsion is not important at neutral pH.[25] The final structures of the produced nanoparticles are shown as a cartoon in Scheme 1, and the results of the particles characterized by DLS and MALDI-SEC are summarized in Table 1. All control nanoparticles have a

Table 1. Characterization of the Control and Nanoparticles: Polymer Gel Content (Weight %), Chain Mass-Average Molecular Weight (M_w) and Number-Average Molecular Weight (M_n), Particle Hydrodynamic Diameter (D_h), and Dispersion Solids Content (SC) (Weight %)

	control nanoparticles			hybrid nanoparticles		
	NP	*P*-NP	*A*-NP	NPT	*P*-NPT	*A*-NPT
polymer gel (wt %)[a]	7	7	7	7	7	7
M_n	6.0×10^4	7.2×10^4	6.5×10^4	8.2×10^4	8.1×10^4	7.2×10^4
M_w/M_n	2.0	1.8	1.7	1.7	1.6	1.8
D_h (nm)	110.6	114.3	117.1	105.7	104.0	99.0
rel. var.	0.016	0.026	0.007	0.015	0.014	0.016
SC (wt %)	34	33	33	27	29	30

[a]Ratio of cross-linked PBMA from NRs to the total PBMA forming the nanoparticles.

polymer gel content of 7 wt %, coming from the fully cross-linked NRs which become incorporated into the final particle structures. The molecular weight of the linear chains is $M_w \approx 1.2 \times 10^5$, both for the dye-labeled and the unlabeled particles. MALDI-SEC measurements revealed that in the case of labeled particles, dyes were attached only to the linear chains (as negligible fluorescence signals were detected at long elution times, where unreacted dyes would appear). Despite the presence of MAA and TEOS, hybrid nanoparticles show the same polymer gel content (7 wt %) and almost the same molecular weight of linear chains ($M_w \approx 1.3 \times 10^5$). This is an indication that no significative branching or network formation inside the NRs occurred during the second polymerization step. In addition, all particles revealed similar sizes, with $D_h \approx 100-120$ nm and low relative variances. It is thus apparent that, despite the silica precursor encapsulation and the MAA copolymerization into the linear chains, the structure and dimensions of the hybrid particles remained similar to those of the polymeric control particles.

3.2. Chain Interdiffusion in Hybrid Films. Dispersions of Phe- and Ant-labeled nanoparticles were mixed in a 1:1 molar ratio, cast into a film, dried inside a closed chamber saturated with water vapor at 30 °C, and annealed at four different temperatures: 80, 90, 100, or 110 °C. The phenanthrene fluorescence decay curves were measured at room temperature for the different films, after annealing during several periods of time. For films prepared from phenanthrene-labeled control particles only (*P*-NP), the decay is monoexponential, with a fluorescence lifetime of $\tau_D = 47$ ns (Figure S1, decay A, in Supporting Information). Films prepared from a 1:1 molar mixture of *P*-NP and *A*-NP show, at zero annealing time, a fluorescence decay curve with just a small deviation from the strictly exponential decay (Figure S1, decay B, in Supporting Information) caused by energy transfer from the donor- to the acceptor-labeled chains located near the interfaces of contiguous particles. After annealing the same *P*-NP + *A*-NP film at 110 °C for 30 min, the donor fluorescence decay is clearly nonexponential (Figure S1, decay C, in Supporting Information), which indicates an increase in energy transfer, thus reflecting the chain interdiffusion across interparticle boundaries.

Figure 1 shows the time evolution of the apparent fraction of the mixture, f_m, calculated using eqs 1 and 2, for two films

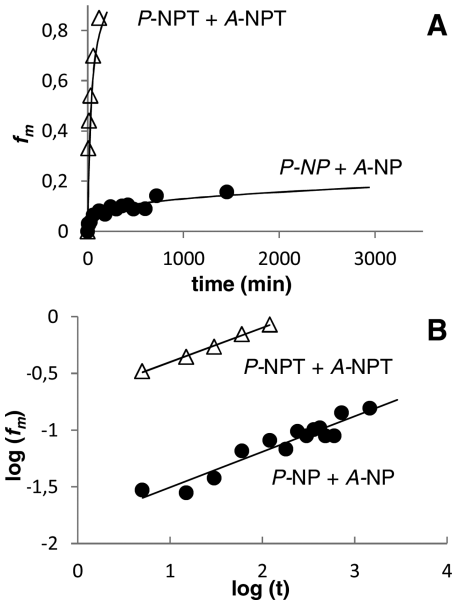

Figure 1. Apparent fraction of mixing, f_m, as a function of annealing time for two 1:1 molar mixtures of control polymer particles, *P*-NP + A-NP (•), and hybrid particles, *P*-NPT + *A*-NPT (Δ), at 80 °C. Linear (A) and logarithmic (B) plots.

annealed at 80 °C. One was cast from a 1:1 molar mixture of control particles, *P*-NP + A-NP (closed symbols), and the other from a 1:1 molar mixture of hybrid particles, *P*-NPT + *A*-NPT (open symbols). We observe that f_m increases with annealing time for both films (Figure 1A), though f_m values are significantly higher and increase faster for films of hybrid nanoparticles (showing a plateau at $f_m > 0.8$ for an annealing time of 100 min, compared to a plateau at $f_m = 0.2$ after 1000 min in the control film). This is a clear indication of a strong plasticizing effect, which in this case can be attributed only to the unreacted TEOS molecules encapsulated in the particles.

We also observe that the f_m plateau value in films of the control particles (Figure 1A) is lower than the reported in literature for nanoparticles of similar dimensions of PBMA linear chains with similar molecular weights.[26−28] This is attributed to both the lower dispersity of the linear chains and the architecture of the particles, which still contain ca. 7 wt % of polymer gel from the NRs.[18]

Figure 1B shows that the logarithmic plots of the same parameters are linear, with similar slopes in both films (0.31 ± 0.06 for the control film and 0.30 ± 0.01 for the hybrid film). This results from the fact that both control and hybrid particles have the same relative amount of polymer gel content and

dx.doi.org/10.1021/la502826r | *Langmuir* 2014, 30, 12345−12353

linear chains with similar molecular weights. In fact, for both films the molecular weight of the linear polymer chains is close to the limit of the Fickian regime ($M_n \approx 2M_e^{PBMA} = 6.4 \times 10^4$, where M_e^{PBMA} is the entanglement molecular weight of PBMA[26]), with a scaling exponent close to 0.5 being expected for both control and hybrid films. Again, the lower values obtained (ca. 0.3) can be explained by the hindering effect of the polymer gel on chain interdiffusion.[18] Apparently, the silica precursors do not interfere with the diffusion mechanism of the chains during annealing at 80 °C.

For control films *P*-NP + *A*-NP, the f_m values obtained at four different annealing temperatures (80, 90, 100, and 110 °C) increase with temperature (Figure S2-A, Supporting Information), reflecting the increase in the rate of chain interdiffusion described in the literature.[29] The slopes obtained in the logarithmic representation (Figure S2B in Supporting Information), 0.31 ± 0.06 (80 °C), 0.28 ± 0.09 (90 °C), 0.3 ± 0.1 (100 °C), and 0.14 ± 0.04 (100 °C), are again very similar, pointing to the same diffusion mechanism at all temperatures.

Figure 2 shows the f_m time evolution obtained at the same four annealing temperatures (80, 90, 100, and 110 °C) for

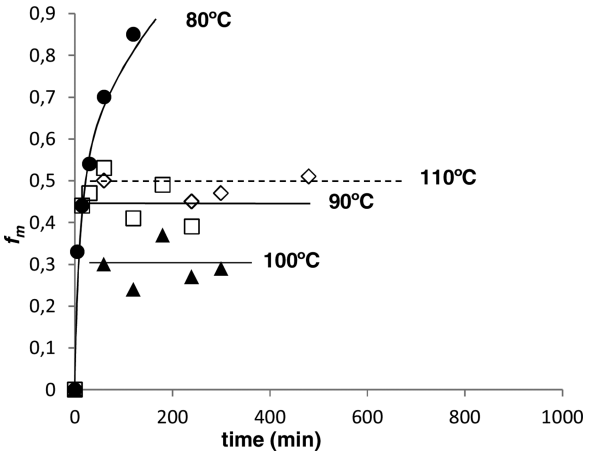

Figure 2. Time evolution of the apparent fraction of the mixture, f_m, in hybrid films, *P*-NPT + *A*-NPT, annealed at 80 (●), 90 (□), 100 (▲), and 110 °C (◇).

hybrid films. In this case, we observe a new tendency, with the f_m plateau values decreasing with temperature between 80 and 100 °C and increasing at 110 °C. This cannot be explained by the interdiffusion of linear PBMA chains, which was previously observed to increase with temperature (Figure S2, Supporting Information).[29]

Above 90 °C the plateaus are reached almost immediately, in contrast to the smooth evolution of f_m at 80 °C. A similar effect was observed by Winnik and coworkers when comparing the time evolution of f_m for two p(BA-*co*-MAA) latexes with and without the *N*-(isobutoxymethyl)acrylamine (IBMA) reactive comonomer.[13] They observed that, while at early stages the interdiffusion rates of the IBMA-containing film and the IBMA-free film were very similar, the f_m value for the IBMA-containing polymer ceased to increase shortly after, which was interpreted as an interruption of polymer chain interdiffusion.

According to both Joanicot et al.[30,31] and Feng et al.,[32] it is accepted that residual water remains inside hydrophobic latex films after the drying stage, either from the original aqueous dispersion or from air moisture, mainly in the boundary region, which is richer in polar groups. When annealed at 80 °C, most of the water molecules tend to remain at their initial location, at the interfaces, because of the small affinity of water for the PBMA chains. A similar situation was described in the literature, where hexamethoxymethyl melamine, a gas previously dissolved in the aqueous medium of the emulsion, also remained at the interfaces of PBMA particles after drying and annealing as a result of immiscibility.[33] TEOS is strongly hydrophobic, remaining homogeneously distributed inside the particles. With residual water concentrating at the interface between particles, TEOS hydrolysis is thus not likely to occur.

Some of the TEOS inside the particles may, however, have reacted with MAA groups during the particle synthesis and emulsion storage because the pH was higher than pK_a(MAA) and therefore the nucleophile $-COO^-$ groups of the MAA units could react with TEOS, resulting in TEOS-MAA side groups.

During annealing, the entropically constrained chains diffuse across the interparticle boundaries to adopt more stable conformations. The TEOS-MAA side groups can be dragged by the chains and reach the interparticle boundaries, where both water molecules and H^+ ions are present (from superficial MAA groups, protonated after the treatment with the ion-exchange resin). Under these circumstances, the TEOS-MAA side groups can be hydrolyzed, subsequently condensing with free TEOS to produce inorganic oligomers grafted to the p(BMA-*co*-MAA) chains through the MAA groups. These reactions did not occur to a large extent at 80 °C; otherwise, the polymer chains' molecular weight would have been substantially increased, thus decreasing the chain mobility as described for branched chains.[23] In conclusion, despite the possibility of some grafting of TEOS to MAA groups, at 80 °C most of the TEOS molecules are expected to remain unreacted and to act as plasticizers, enhancing chain interdiffusion.

For films annealed at higher temperatures, water molecules diffuse into the PBMA particles more easily and can hydrolyze the encapsulated TEOS molecules in the presence of protons from the MAA groups. Hydrolyzed TEOS can react both with other TEOS molecules (forming silica domains) and with TEOS-MAA side groups, increasing the length of the inorganic grafted chains. Both processes hinder chain interdiffusion, in the extreme, forming silica domains that eventually stop chain diffusion. Another possibility is the condensation of a growing inorganic chain grafted to MAA with a TEOS-MAA side group of a neighboring PBMA chain to form an inorganic bridge between two distinct polymer chains, also preventing chain diffusion.

Indeed, the extent of water diffusion (which increases with the annealing temperature) determines the extent of hydrolysis and condensation reactions of TEOS, which lead to the formation of hybrid silica−polymer cross-links, and ultimately stops polymer interdiffusion. The plateaus observed for the higher annealing temperatures in f_m versus time plots no longer correspond to full chain interdiffusion as in the control films but to the maximum mixing obtained before diffusion is stopped as a result of the formation of organic−inorganic cross-linked structures. The highest f_m plateau obtained at 110 °C is due to faster chain interdiffusion at this temperature, with more chains crossing the interface between particles before extensive cross-linking occurs.

Apparent mean diffusion coefficients, D_{app}, can be used to characterize the labeled polymer chains' diffusive transport during film formation.[34] These coefficients are determined by fitting f_m data to a Fickian diffusional model,[35] assuming that f_m

dx.doi.org/10.1021/la502826r | *Langmuir* 2014, 30, 12345−12353

is close to the real fraction of mass that has diffused across the interface. Note that D_{app} values are not real center-of-mass diffusion coefficients, but are expected to be proportional to these values for $f_m < 0.7$.[22]

The plots of D_{app} values for both control and hybrid films as a function of f_m at four annealing temperatures (80, 90, 100, and 110 °C) show that D_{app} values are almost independent of f_m (Figure 3), a consequence of the low dispersity of the linear chains.[18] The averaged D_{app} values for each film (Table S2, Supporting Information) are presented in Figure 4 as a function of annealing temperature. It is clear that whereas the mean $\langle D_{app} \rangle$ values increase with annealing temperature for the control films, they decrease for the hybrid ones because of the larger extent of sol−gel reactions. At 80 °C, the determined $\langle D_{app} \rangle$ for the hybrid film is much higher than for the control film. As mentioned before, diffusion is enhanced by the plasticizing effect of unreacted TEOS. The same trend is observed at 90 °C, but with a smaller difference between the two $\langle D_{app} \rangle$ values. In fact, the higher chain interdiffusion rate is balanced by the larger extent of the sol−gel reactions, promoted by the increased mobility of water, which decreases chain interdiffusion as a result of the formation of organic−inorganic domains. At 100 °C both films present similar averaged apparent mean diffusion coefficients.

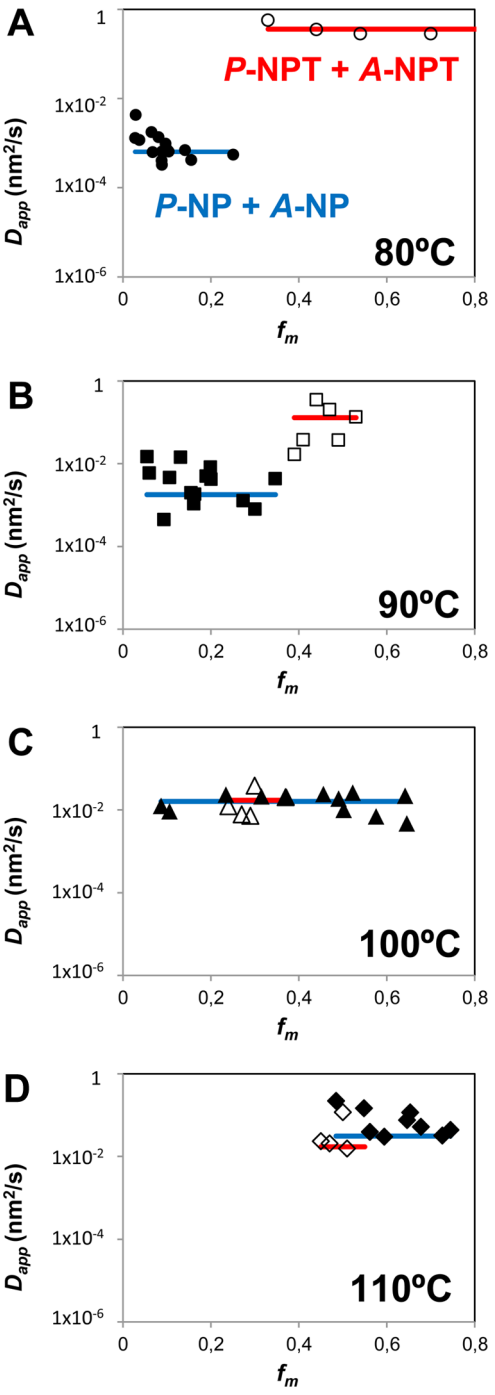

Figure 3. Apparent mean diffusion coefficients, D_{app}, as a function of the fraction of the mixture, f_m, for films formed from control particles, *P*-NP + *A*-NP (closed symbols) and from hybrid particles, *P*-NPT + *A*-NPT (open symbols), at four different annealing temperatures: 80 (A), 90 (B), 100 (C), and 110 °C (D). Horizontal lines indicate the average D_{app} values (control particles in blue, hybrid particles in red).

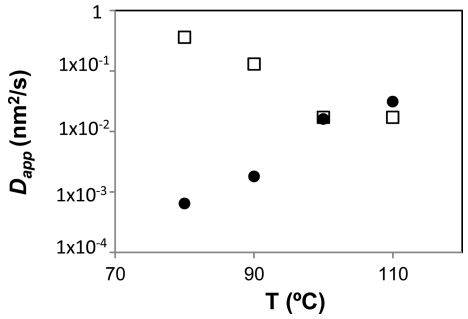

Figure 4. Time-averaged D_{app} variation with the annealing temperature on the control films (●) and the hybrid films (□).

3.3. Formation of Hybrid Structures. The formation of inorganic−organic structures during the annealing of the hybrid films was studied by DRIFT spectroscopy of unlabeled hybrid films annealed at 80 and 110 °C. In Figure 5A, the DRIFT spectra of a hybrid film formed from nonfluorescent particles, NPT, before and after annealing at different temperatures, for different periods, are compared to that of a control film, NP. All spectra show the typical features of a PBMA film. In the 4000−2000 cm^{-1} region (Figure 5B), the spectra are dominated by the bands associated with the CH_2 and CH_3 stretching modes. The strong νC=O band, centered at 1725 cm^{-1}, remains almost invariant and was used to normalize the spectra. The 1600−700 cm^{-1} range (Figure 5C) contains the most intense bands, related to the C−O stretching modes. The higher-wavenumber region in this range shows the C−H deformation bands, and the lower-wavenumber region contains bands from the C−H rocking modes, along with the νC−C vibrational band. The 575−425 cm^{-1} region (Figure 5D) displays the C−O deformation-related bands and will be discussed in detail below.[36]

The presence of unreacted TEOS in the hybrid films, before and after thermal annealing at 80 °C, is apparent from the presence of a distinct band at 478 cm^{-1} (δO−C−C, Figure 5D), resulting from nonhydrolyzed ethoxy groups and a small feature observed at 804 cm^{-1} ($\nu_{as}SiO_4$, Figure 5C), absent in the control film spectrum.[37] Besides, the 1200−900 cm^{-1} region is more intense in the hybrid films because of the overlapping of the PBMA spectral features with the intense TEOS bands at 1105 (ν_{as}Si−O), 1082 (ν_{as}C−O), and 964 ($\rho_s CH_3$) cm^{-1}. These observations confirm the encapsulation of unreacted TEOS inside the particles and their long-term stability during storage. They are also consistent with the

dx.doi.org/10.1021/la502826r | Langmuir 2014, 30, 12345−12353

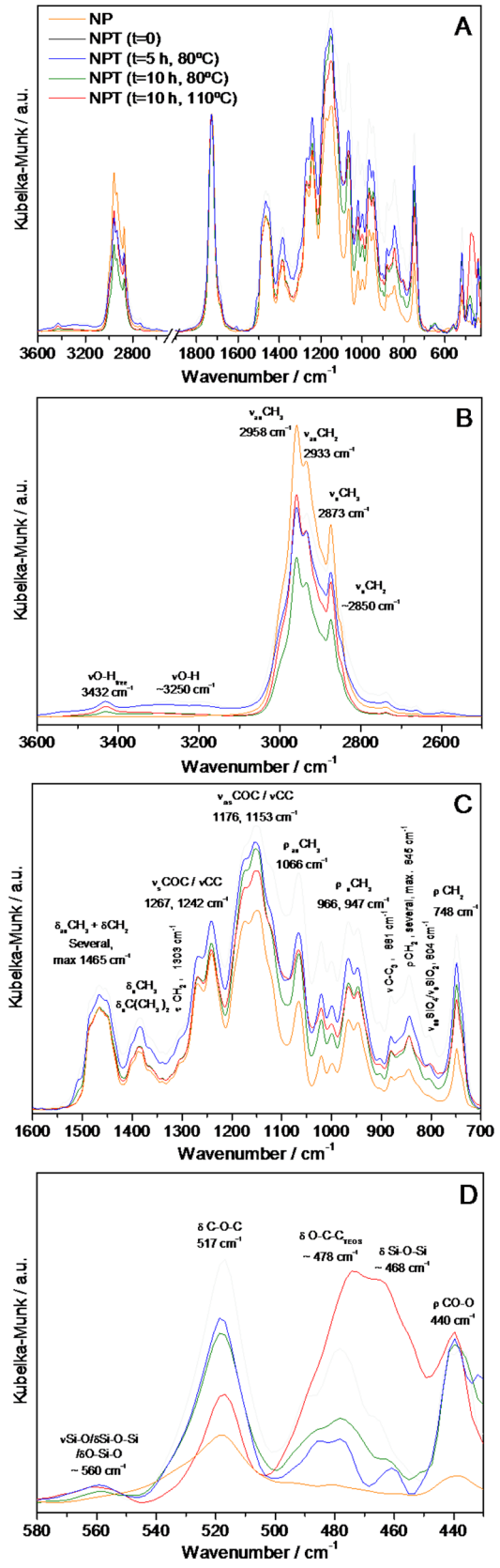

Figure 5. Comparison of the DRIFT spectra, normalized to the νC=O band at ~1725 cm^{-1}, of a hybrid film, NPT, before annealing (black), after 5 h of annealing at 80 °C (blue), and after 10 h of annealing at 80 °C (green) and at 110 °C (red) with a control film, NP (orange) (A). Amplifications of relevant spectral regions B–D.

proposed plasticizing effect of unreacted TEOS at low annealing temperatures.

Another difference between the NP and NPT spectra is the presence of a broad hydroxyl-related band centered at ~3250 cm^{-1} (νO–H, Figure 5B) whose intensity decreases with annealing, disappearing after 10 h of thermal treatment at 80 °C. This band is most probably related to the presence of ethanol (eliminated during TEOS hydrolysis and condensation), which disappears upon annealing as a result of evaporation. The 1600–700 cm^{-1} spectral region (Figure 5C) confirms this assignment: upon annealing at 80 °C and with increasing annealing time, all of the CH_2- and CH_3-related bands decrease, and for longer annealing times, the spectra of the NP and NPT films almost overlap in the CH deformation region (1600–1200 cm^{-1}). However, the contribution of silanol groups to the νO–H band cannot be ruled out. They could also be present and decrease in number with condensation occurring during annealing.

The role of TEOS during annealing can also be inferred from Figure 5C, where the most intense band in all of the spectra (ν_{as}COC) is higher for the hybrid films than for the control film as a result of partial overlap with TEOS' most intense bands, ν_{as}C–O and ν_{as}Si–O (at 1082 and 1103 cm^{-1} respectively).[37] The relative intensity of this band decreases with annealing time and temperature, indicating TEOS hydrolysis. The same can be concluded from the decrease in $\nu_{as}SiO_4$, centered at 804 cm^{-1}, with annealing at 80 °C. Despite the indications of TEOS reaction at this temperature, there is no unambiguous proof of silica formation by condensation, even after 10 h of annealing. Silica has an intense spectrum with typical features of ν_{as}Si–O–Si and ν_sSi–O–Si that would appear precisely at 1100–100 and 804 cm^{-1}. Thus, if silica were forming by condensation and TEOS were acting as a cross-linker, then Si–O–Si-related bands would replace TEOS bands and the intensity decrease observed would not be so sharp. However, upon annealing at 110 °C, there are clear indications of silica formation. These are the appearance of a medium-intensity band at 468 cm^{-1}, assigned to the Si–O–Si deformation band (δSi–O–Si,[37] Figure 5D), which replaces the 478 cm^{-1} TEOS band, and the fact that the decrease in the 804 cm^{-1} band intensity upon annealing is not so sharp because the $\nu_{as}SiO_4$ TEOS band is being partially replaced by the ν_sSiOSi silica band. Unfortunately, because of the low MAA content (ca. 0.8 wt %) it is not possible to follow the MAA-TEOS side group formation by DRIFT. The condensation of TEOS was evident in the CP-MAS ^{29}Si NMR spectra (Bruker, 400 MHz) of films cast from particles with twice the amount of TEOS as NPT and annealed during 10 h at 110 °C. The spectra show some of the characteristics peaks of condensed TEOS (with chemical shifts relative to Si$(CH_3)_4$): Q^2 (−91 ppm), Q^3 (−102 ppm), and Q^4 (−109 and −115 ppm) (Figure S3 of the Supporting Information). The intensity of the signals show that Si participates in a 3D network because the Q^2 signal is relatively small.[17] Analytical TEM (EDS) shows that silicon is uniformly distributed in the film (Figure S4 in the Supporting Information), proving that TEOS was initially homogeneously distributed inside the latex particles.

These results clearly show that by annealing the NPT films at 110 °C, TEOS molecules undergo hydrolysis and condensation, originating SiO_2 domains that increase the length of the inorganic chains grafted to the acrylic acid groups of the polymer chains and eventually form inorganic bridges between p(BMA-*co*-MAA) chains. This is probably due to the highest

dx.doi.org/10.1021/la502826r | *Langmuir* 2014, 30, 12345–12353

water mobility at 110 °C, which allows its diffusion into the p(BMA-*co*-MAA) particles. On the contrary, at lower temperatures, water mobility is lower and most TEOS molecules remain unreacted, acting as plasticizers during film formation. Such a mechanism explains the decrease in the f_m plateau with increasing temperature in the hybrid films (Figure 2), which opposes the expected increase in chain interdiffusion with temperature as well as the decrease in the mean diffusion coefficients for hybrid films, contrary to what is observed for NP films (Figure 4).

3.4. Film Resistance to Solvents. FRET and DRIFT experiments provided information on the extent of chain interdiffusion across the particle interfaces and on the organic–inorganic cross-link formation during film annealing. However, neither the diffusion experiments nor the chemical characterization of the films during annealing allows, by itself, the direct evaluation of the degree of healing and cohesion in the film. Here, the effect of healing was studied by swelling NPT thick hybrid films of ca. 1 g and roughly the same shape and dimensions (previously annealed at the desired temperature for 90 min) in THF, a good solvent for PBMA. The films were washed with THF for 45 min, dried at room temperature, and weighed. The fraction of remaining macroscopic gel, RMG wt %, was calculated as the ratio of the mass of the dried film to the corresponding initial mass (Table 2).

Table 2. Weight Fractions of the Hybrid Films (NPT) that Remained after Washing with THF for 45 Minutes[a]

annealing temperature (°C)	RMG (wt %)
80	56
90	78
100	55
110	46

[a]All films were previously annealed during 90 min at the mentioned annealing temperatures.

We expect that the films with the best healing properties are those annealed at a temperature that is high enough to promote rapid chain interdiffusion but low enough to prevent silica network formation, which can compete with the diffusion process. In fact, the best resistance to THF corresponds to the intermediate annealing temperature of 90 °C. This is in agreement with both FRET and DRIFT results, which indicated that at 90 °C the extent of sol–gel reactions is higher than at 80 °C and chain interdiffusion is larger than at 110 °C. However, at 80 °C the sol–gel reactions are too slow to efficiently cross-link the chains that diffuse across the interface between particles. At 110 °C, the sol–gel reactions occur almost instantaneously, preventing further chain interdiffusion (Scheme S1, Supporting Information).

Additional healing tests performed with a set of films cast from particles similar to NPT but produced without MAA, leading to % RMG values of ca. 50% of those obtained for the NPT films at annealing temperatures of both 80 and 110 °C. This indicates that the MAA groups do make a considerable contribution to the integrity of the films. Thus, although the NMR and DRIFT experiments were not sensitive enough to follow the reactions of the MAA groups, the results of the healing tests show that cross-linking reactions between the polymer chains and silica domains must have occurred through the MAA groups.

4. CONCLUSIONS

In this work hybrid emulsions of PBMA nanoparticles containing TEOS were produced and observed to be stable during very long times. These emulsions were used to produce hybrid films, which were dried at 30 °C (slightly above the T_g of PBMA) and annealed at several temperatures (from 80 to 110 °C). Both chain interdiffusion and silica formation were affected by the temperature and were followed during annealing by FRET and DRIFT, respectively.

We found that TEOS acts as a "smart" molecule. Although it remains mostly unreacted during the emulsion polymerization (the resulting particle dispersion, kept at pH 7, is stable for very long times), during film formation TEOS plays an active double role: it can act both as a plasticizer for the polymer chains and as a cross-linking agent, forming a hybrid network with the polymer. The weight of the two roles changes with the temperature at which the film is annealed because the two phenomena depend differently on temperature. At 80 °C, the reactivity of TEOS is low and it acts as a plasticizer for a long time before reacting. At higher temperatures water diffusion increases, promoting sol–gel reactions and the formation of either hybrid or even pure silica domains that slow down polymer diffusion and eventually avoid the formation of a fully developed film.

Film healing was evaluated through chemical resistance tests using THF, a good solvent for the polymer. The best results were observed at 90 °C, where TEOS could both plasticize the chains (contributing to chain interdiffusion across particle boundaries) and react with the MAA groups of the polymeric chains (anchoring the ends of the chains bridging the interfaces between particles), thus avoiding chain pull-out by the action of the solvent.

This novel strategy has the advantage of allowing us to tune the diffusion/cross-linking in the forming film without using VOCs; not only is the coalescing aid not released from the film, but it is used as a cross-linker to increase the film mechanical properties. This is an extremely attractive approach to producing water-borne high-performance environmental friendly binders for paints and coatings, with very good mechanical properties and chemical resistance and nearly zero VOC content.

■ ASSOCIATED CONTENT

Supporting Information

Recipes used for the synthesis of the nanoparticles. Fluorescence decay curves. Plots of the apparent fraction of the mixture with annealing time for control films. Averaged D_{app} at each temperature. CP-MAS ^{29}Si NMR spectrum of an annealed NPT film. TEM images of an annealed NPT film. Cartoon illustrating two adjacent cells of films formed by annealing during film disintegration by THF. Long-term stability of the hybrid particles. DRIFT spectra of lyophilized particles of pure PBMA particles and TEOS-containing PBMA particles stored for different periods of time. Amplification of the 580–450 cm^{-1} spectral region in the DRIFT spectra of lyophilized particles of pure PBMA particles and TEOS-containing PBMA particles stored for different periods of time. This material is available free of charge via the Internet at http://pubs.acs.org.

AUTHOR INFORMATION

Corresponding Authors

*E-mail: susana.goncalves@estsetubal.ips.pt. Tel: +(351) 966341892.

*E-mail: farinha@tecnico.ulisboa.pt. Tel: +(351) 218419221.

Notes

The authors declare no competing financial interest.

ACKNOWLEDGMENTS

We thank Prof. Laura Ilharco for helpful discussions on the DRIFT results and Dr. Tânia Ribeiro for the TEM measurements. This work was supported by Fundação para a Ciência e a Tecnologia (FCT, Portugal) through project RECI/CTM-POL/0342/2012.

REFERENCES

(1) Keddie, J. L.; Routh, A. F. *Fundamentals of Latex Film Formation: Processes and Properties*; Springer: New York, 2010.

(2) Sheetz, D. P. Formation of Films by Crying of Latex. *J. Appl. Polym. Sci.* **1965**, *9*, 3759−3773.

(3) Eckersley, S. T.; Rudin, A. Mechanism of Film Formation from Polymer Latexes. *J. Coat. Technol.* **1990**, *62*, 89−100.

(4) Keddie, J. L. Film Formation of Latex. *Mater. Sci. Eng.* **1997**, *21*, 101−170.

(5) Winnik, M. A. Latex Film Formation. *Curr. Opin. Colloidal Interface Sci.* **1997**, *2*, 192−199.

(6) Steward, P. A.; Hearn, J.; Wilkinson, M. C. An Overview of Polymer Latex Film Formation and Properties. *Adv. Colloid Interface Sci.* **2000**, *86*, 195−267.

(7) Mohammadi, N.; Klein, A.; Sperling, L. H. Polymer-Chain Rupture and the Fracture-Behaviour of Glassy Polystyrene. *Macromolecules* **1993**, *26*, 1019−1026.

(8) Kim, K. D.; Sperling, L. H.; Klein, A.; Hammouda, B. Reptation Time, Temperature, and Cosurfactant Effects on the Molecular Interdiffusion Rate During Polystyrene Latex Film Formation. *Macromolecules* **1994**, *27*, 6841−6850.

(9) Aradian, A.; Raphaël, E.; de Gennes, P.-G. Scaling Theory of the Competition Between Interdiffusion and Cross-Linking at Polymer Interfaces. *Macromolecules* **2002**, *35*, 4036−4043.

(10) Pham, H. H.; Farinha, J. P. S.; Winnik, M. A. Cross-Linking, Miscibility, and Interface Structure in Blends of Poly(2-ethylhexyl methacrylate) Copolymers. *Macromolecules* **2000**, *33*, 3850−3860.

(11) Bufkin, B. G.; Grawe, J. R. Survey of Applications, Properties, and Technology of Crosslinking Emulsions. *J. Coat. Technol.* **1978**, *50*, 41−55; **1978**, *50*, 67−83; **1978**, *50*, 83−109; **1978**, *50*, 70−100; **1978**, *50*, 65−96; **1979**, *51*, 34−67.

(12) Winnik, M. A. Interdiffusion and Crosslinking in Thermoset Latex Films. *J. Coat. Technol.* **2002**, *74*, 49−63.

(13) Liu, R.; Winnik, M. A.; Di Stefano, F.; Venkatesan, J. Interdiffusion vs Cross-Linking Rates in Isobutoxyacrylamide-Containing Latex Coatings. *Macromolecules* **2001**, *34*, 7306−7314.

(14) Zosel, A.; Ley, G. Influence of Cross-Linking on Structure, Mechanical-Properties, and Strength of Latex Films. *Macromolecules* **1993**, *32*, 2222−2227.

(15) Pham, H.; Winnik, M. A. Synthesis, Characterization, and Stability of Carbodiimide Groups in Carbodiimide-Functionalized Latex Dispersions and Films. *J. Polym. Sci., Part A: Polym. Chem.* **2000**, *38*, 855−869.

(16) Wicks, Z. W., Jr.; *Film Formation*; Federation Series on Coatings Technology; Federation of Societies for Coatings Technology: Philadelphia, PA, 1986.

(17) Brinker, C. J.; Scherer, G. W. *Sol-Gel Science: The Physics and Chemistry of Sol-Gel Processing*; Academic Press: Boston, MA, 1990.

(18) Piçarra, S.; Afonso, C. A. M.; Kutreva, V. B.; Fedorov, A.; Martinho, J. M. G.; Farinha, J. P. S. The Influence of Nanoparticle Architecture on Latex Film Formation and Healing Properties. *J. Colloid Interface Sci.* **2012**, *368*, 21−33.

(19) Afonso, C. A. M.; Farinha, J. P. S. Synthesis of 4-Aryl-butylamine Fluorescent Probes. *J. Chem. Res., Synop.* **2002**, *11*, 584−587.

(20) Cummins, H. Z.; Pusey, P. N. In *Photon Correlation Spectroscopy and Velocimetry*, Cummins, H. Z.; Pike, E. R., Eds.; Plenum Press: New York, 1977.

(21) Farinha, J. P. S.; Martinho, J. M. G.; Pogliani, L. Non-Linear Least-Squares and Chemical Kinetics. An Improved Method to Analyze Monomer-Excimer Decay Data. *J. Math. Chem.* **1997**, *21*, 131−139.

(22) Farinha, J. P. S.; Martinho, J. M. G. Ressonance Energy Transfer in Polymer Nanodomains. *J. Phys. Chem. C* **2008**, *112*, 10591−10601.

(23) Farinha, J. P. S.; Wu, J.; Winnik, M. A.; Farwaha, R.; Rademacher, J. Polymer Diffusion in Gel-Containing Poly(vinyl acetate-co-dibutyl maleate) Latex Films. *Macromolecules* **2005**, *38*, 4393−4402.

(24) Chen, S.-A.; Lee, S.-T. Seeded Latex Polymerizations − Studies on the Particle Growth. Mechanism of Latex Particles. *Polymer* **1992**, *33*, 1437−1444.

(25) Arriagada, F. J.; Osseo-Asare, K. Controlled hydrolysis of tetraethoxysilane in a nonionic water-in-oil microemulsion: a statistical modelo f sílica nucleation. *Colloids Surf., A* **1999**, *154*, 311−326.

(26) Wang, Y.; Winnik, M. A. Polymer Diffusion across Interfaces in Latex Films. *J. Phys. Chem.* **1993**, *97*, 2507−2515.

(27) Liu, Y.; Schroeder, W. F.; Haley, J. C.; Lau, W.; Winnik, M. A. Effect of Branching on Polymer Diffusion in Branched Poly(butyl methacrylate) Latex Films. *Macromolecules* **2009**, *41*, 9104−9111.

(28) Odrobina, E.; Winnik, M. A. Influence of Entanglements on the Time Dependence of Mixing in Nonradiative Energy Transfer Studies of Polymer Diffusion in Latex Films. *Macromolecules* **2001**, *34*, 6029−6038.

(29) Ye, S.; Farinha, J. P. S.; Oh, J.K.; Winnik, M.A.; Wu, C. Polymer Diffusion in PBMA Latex Films using a Polymerizable Benzophenone Derivative as an Energy Transfer Acceptor. *Macromolecules* **2003**, *36*, 8749−6769.

(30) Chevalier, Y.; Pichot, C.; Graillant, C.; Joanicot, M.; Wong, K.; Maquet, J.; Lindner, P.; Cabane, B. Film Formation with Latex-Particles. *Colloid Polym. Sci.* **1992**, *270*, 806−821.

(31) Joanicot, M.; Wong, K.; Cabane, B. Interdiffusion in Cellular Latex Films. *Macromolecules* **1996**, *29*, 4976−4984.

(32) Feng, J.; Winnik, M. A. Effect of Water on Polymer Diffusion in Latex Films. *Macromolecules* **1997**, *30*, 4324−4331.

(33) Winnik, M. A.; Pinenq, P.; Krüger, C.; Zhang, J.; Yaneff, P. V. Crosslinking vs. Interdiffusion Rates in Melamine-Formaldehyde Cured Latex Coatings: A Model for Waterborne Automotive Basecoat. *J. Coat. Technol.* **1999**, *71*, 47−60.

(34) Farinha, J. P. S.; Vorobyova, O.; Winnik, M. A. An Energy Transfer Study of the Interface Thickness in Blends of Poly(butyl methacrylate) and Poly(2-ethylhexyl methacrylate). *Macromolecules* **2000**, *33*, 5863−5873.

(35) Crank, J. *Mathematics of Diffusion*; Clarendon Press: Oxford, U.K., 1975.

(36) Socrates, G. *Infrared and Raman Characteristic Group Frequencies, Tables and Charts*, 3rd ed.; John Wiley & Sons, Ltd: Chichester, U.K., 2004.

(37) Matos, M.; Ilharco, L. The Evolution of TEOS to Silica-Gel and Glass by Vibrational Spectroscopy. *J. Non-Cryst. Solids* **1992**, *147−148*, 232−237.